Cryo-EM structure of MsbA in saposin-lipid nanoparticles (Salipro) provides insights into nucleotide coordination

Dominique-Maurice Kehlenbeck[1,2,3,4], Daouda A.K. Traore[3,4,5,6], Inokentijs Josts[1,2], Simon Sander[1,2], Martine Moulin[3,4], Michael Haertlein[3,4], Sylvain Prevost[7], V. Trevor Forsyth[3,4,5] and Henning Tidow[1] (iD)

1 The Hamburg Advanced Research Center for Bioorganic Chemistry (HARBOR), Germany
2 Department of Chemistry, Institute for Biochemistry and Molecular Biology, University of Hamburg, Germany
3 Life Sciences Group, Institut Laue–Langevin, Grenoble, France
4 Partnership for Structural Biology (PSB), Grenoble, France
5 Faculty of Natural Sciences, Keele University, UK
6 Faculté des Sciences et Techniques, Université des Sciences, des Techniques et des Technologies de Bamako (USTTB), Bamako, Mali
7 Large Scale Structures Group, Institut Laue–Langevin, Grenoble, France

The ATP-binding cassette transporter MsbA is a lipid flippase, translocating lipid A, glycolipids, and lipopolysaccharides from the inner to the outer leaflet of the inner membrane of Gram-negative bacteria. It has been used as a model system for time-resolved structural studies as several MsbA structures in different states and reconstitution systems (detergent/nanodiscs/peptidiscs) are available. However, due to the limited resolution of the available structures, detailed structural information on the bound nucleotides has remained elusive. Here, we have reconstituted MsbA in saposin A–lipoprotein nanoparticles (Salipro) and determined the structure of ADP-vanadate-bound MsbA by single-particle cryo-electron microscopy to 3.5 Å resolution. This procedure has resulted in significantly improved resolution and enabled us to model all side chains and visualise detailed ADP-vanadate interactions in the nucleotide-binding domains. The approach may be applicable to other dynamic membrane proteins.

Introduction

Lipid asymmetry between the two leaflets of a bio-membrane is fundamental for cellular life [1,2] and often requires trans-bilayer movement of lipids facilitated by specific flippases [3,4]. MsbA is an ATP-binding cassette (ABC) exporter located in the cytoplasmic membrane of Gram-negative bacteria, where it acts as a lipid flippase, translocating lipid A, glycolipids and lipopolysaccharides (LPS) from the inner to the outer leaflet [5,6]. In addition, it can also function as a multidrug-resistance transporter by exporting various hydrophobic small molecules [7].

MsbA is a prototypical homodimeric ABC transporter composed of two transmembrane domains (TMD; containing six transmembrane helices each) and two nucleotide-binding domains (NBD) [8,9]. The conformational cycle of MsbA follows a "power stroke" mechanism [10]. It is triggered by ATP binding to the NBDs, followed by NBD dimerisation, ATP hydrolysis and subsequent NBD dissociation [9], all of them coupled to movements of the transmembrane helices switching between inward-facing, occluded, and outward-facing conformations. The conformational flexibility of MsbA has been demonstrated by a variety of biophysical techniques, including luminescence resonance energy transfer [11], electron spin resonance spectroscopy [12], crosslinking [13], electron microscopy [14] and molecular dynamics simulations [15]. The well-characterized structural transitions of MsbA occur in the millisecond timescale, making MsbA a model system for time-resolved structural studies [small-angle X-ray scattering (SAXS)] of integral membrane proteins (IMPs) [16, 17].

Several MsbA structures have been determined in different conformational states, using various reconstitution systems, including crystal structures in detergent [8,18–20] as well as single-particle cryogenic electron microscopy (cryo-EM) structures in MSP1D1 nanodiscs [9] or peptidiscs [21]. While these structures provide ample insights into LPS recognition and conformational transitions during the lipid A transport pathway as well as potential inhibition modes of MsbA, details about nucleotide coordination are limited.

Saposin-lipid nanoparticles (Salipro) have been recently introduced as a flexible reconstitution system for IMP [22]. The system uses the lipid-binding protein Saposin A (SapA) to form a discoidal scaffold to provide a lipidic environment for incorporated IMPs [22–24]. Salipro reconstitution works for most lipids, is independent of the size of the incorporated IMP, often results in high activity of the IMP and has been successfully used in a number of cryo-EM structures [25–29].

Here, we report the 3.5 Å resolution cryo-EM structure of Salipro-reconstituted MsbA (from *Escherichia coli*) in an ADP-vanadate(Vi)-bound state. The structure shows MsbA in an occluded conformation with dimerized NBDs and allows clear visualization of the bound nucleotides.

Results and Discussion

Overall structure of MsbA (ADP-Vi) in Salipro

MsbA from *E. coli* was purified from *E. coli* C43 cells in dodecyl maltoside (DDM) detergent and reconstituted into Salipro using 1-palmitoyl-2-oleoyl-glycero-3-phosphocholine (16:0–18:1 PC) (POPC) as lipid (Fig. 1A). This procedure resulted in a monodisperse sample with significantly higher ATPase activity (and stability) compared to the detergent sample and similar activity compared to MsbA reconstituted in MSP1D1 nanodiscs [9,30], indicating that a lipidic environment as provided by nanodisc or Salipro carrier systems is beneficial for structural studies of MsbA.

Orthovanadate can be used to mimic the transition state after ATP hydrolysis (but before phosphate release) by trapping the Mg^{2+}-ADP-Vi complex in the catalytic sites. In this transition state, the stability of Salipro-reconstituted MsbA is significantly increased compared to apo MsbA. While the melting transition midpoint is 53 °C for apo MsbA, it increases to 62 °C for the Mg^{2+}-ADP-Vi-bound complex and to 71 °C for MsbA (ATPγS) (Fig. 1B). Salipro-reconstituted MsbA also retained its specific activity (Fig. 1C).

Using SAXS we have detected significant differences between apo and ADP-vanadate bound MsbA in Salipro in the mid-q region from 0.5 to 3 nm^{-1} (Fig. 1D), which are similar to the X-ray scattering differences of MsbA in nanodiscs [17]. The distance distribution plots show very similar curve progressions and also the values of the radius of gyration (R_g) and maximum dimension (D_{max}) are almost identical (Table 1), indicating that the differences in the scattering reflect internal structural rearrangements. These results show that Salipro-reconstituted MsbA can indeed be trapped in a distinct conformational state by adding Mg^{2+}-ADP-Vi.

Based on the increased thermal stability of Mg^{2+}-ADP-Vi bound complex incorporated in Salipro, we set out to determine its structure using cryo-EM. We hypothesized that this structure would result in a high resolution and highlight key residues involved in
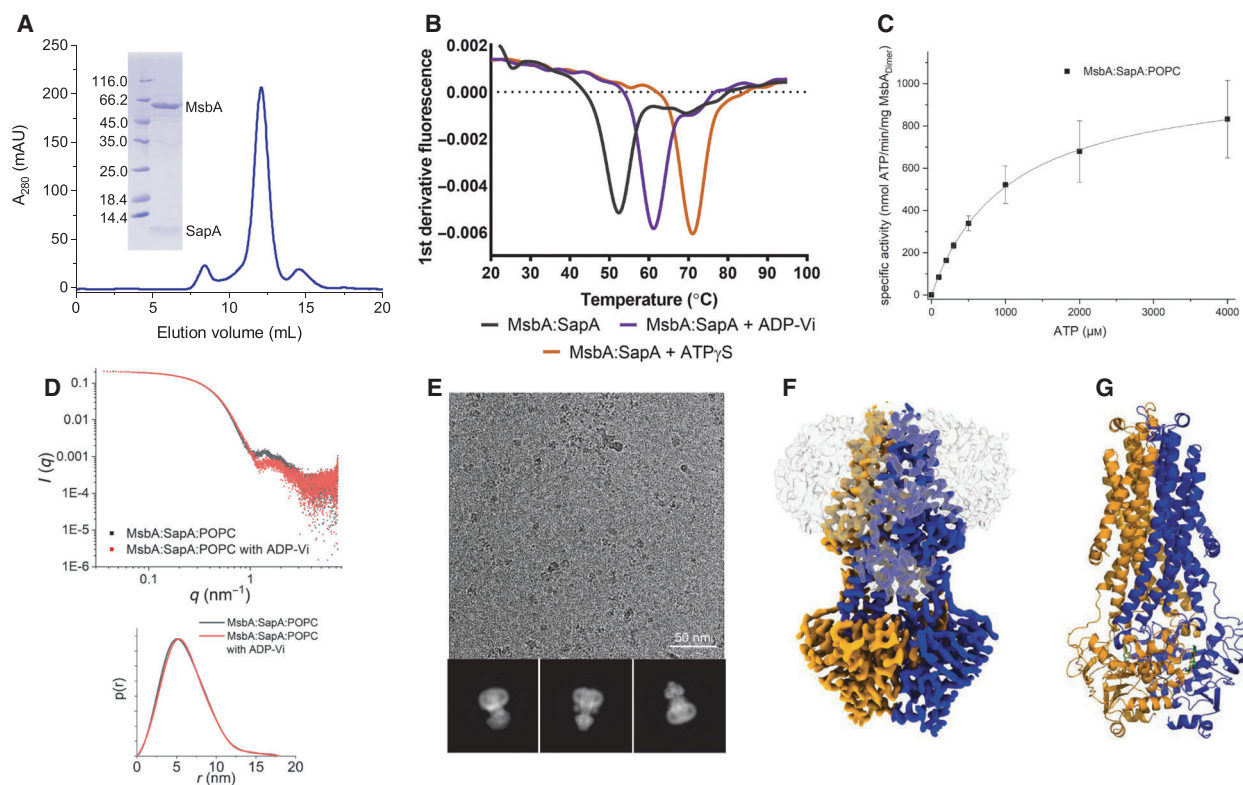
Fig. 1. Characterization and cryo-EM of Salipro-embedded MsbA. (A) SEC profile and corresponding SDS/PAGE gel illustrating MsbA reconstitution into Salipro. (B) Stabilization of Salipro-reconstituted MsbA by ADP-Vi. nDSF thermal melt profiles are shown for apo MsbA (grey), MsbA +ADP-Vi (violet) and MsbA + ATPγS (orange), indicating a significant stabilization of MsbA. Measurements were performed in triplicates. (C) Specific activity of Salipro-reconstituted MsbA measured by the Baginski assay. The maximal reaction speed (V_{max}) of MsbA in Salipro with the lipid POPC is 1110 ± 292 nmol ATP·min^{-1}·mg^{-1} enzyme and the Michaelis constant (K_m) is 1050 ± 289 μM. The experiments were performed as biological triplicates at RT with errors shown as $\pm$ SEM. (D) Comparison of SAXS profiles of MsbA in Salipro in the apo state (black) and with ADP-vanadate (red). Scattering shows significant differences in the mid q-range, indicating structural differences between the two states of MsbA. Distance distribution plots indicating that the differences in the scattering reflecting internal structural rearrangements. (E) Representative cryo-EM image and selected 2D averages of Salipro-embedded MsbA. Box dimension of 2D averages: 183 Å. (F) Surface representation of the MsbA 3D reconstruction, filtered to 3.5 Å resolution. MsbA subunits are coloured orange and blue and the Salipro carrier system is shown as a grey outline. (G) Ribbon diagram of MsbA embedded in Salipro with the subunits coloured in orange and blue. Structure figures were prepared using UCSF Chimera [52] and PYMOL (Schrödinger Inc., New York, NY, USA).

Table 1. SAXS analysis of MsbA incorporated into Salipro with and without ADP-Vi

Sample	R_g (Å)	D_{max} (nm)
MsbA:SapA:POPC	46.5 ± 0.02	18.0
MsbA:SapA:POPC with ADP-Vi	46.6 ± 0.02	18.0

nucleotide binding, thus filling a gap in our knowledge of this important ABC transporter. We selected Salipro-reconstitution with POPC as lipid to collect cryo-EM data on the basis of the high stability and activity of the sample [30] and the potential to combine them with stealth carrier SANS data [31]. In order to remove junk particles picked from the micrographs, we performed two rounds of 2D classifications (Fig. 1E). This was followed by two rounds of 3D classifications to obtain a homogenous set of particles for the final 3D reconstruction. After further refinements and masking out the Salipro disc, a final map with a resolution of 3.5 Å at gold standard FSC 0.143 (Figs 1F,G, 2 and 3) was obtained.

The local resolution filtered map is presented in Fig. 3. At this resolution, it was possible to resolve the structure for the transmembrane helices as well as the NBDs including the side chains. Overall, the transition state structure of MsbA (with Mg^{2+}-ADP-Vi) in Salipro presented here resembles an occluded conformation similar to the structure in nanodiscs [9] but significantly different from the outward open conformation observed in the crystal structure [8] (Fig. 1F, G).

Data processing pipeline
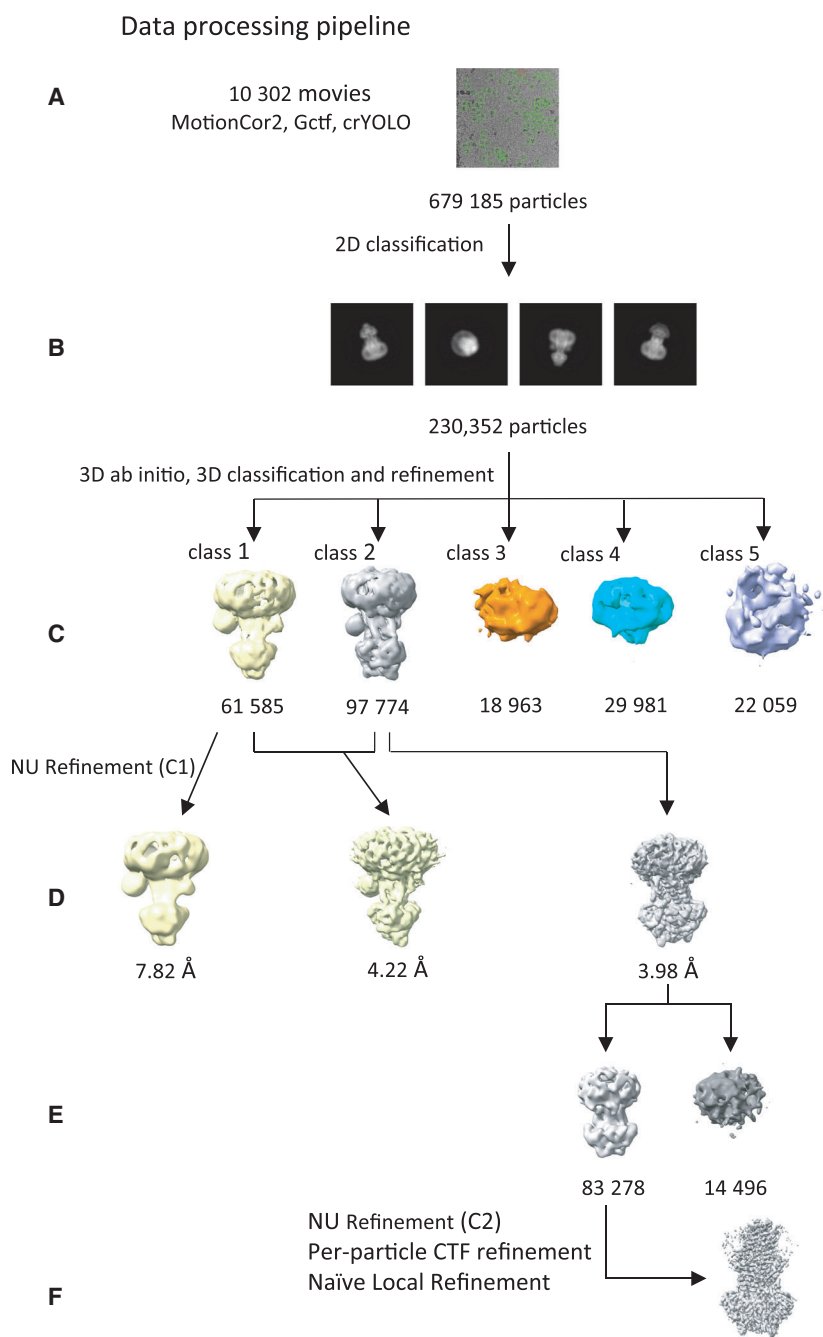
Fig. 2. Image processing workflow for ADP-vanadate bound MsbA in Salipro. (A) Starting with 10 302 movies, the pre-processing, including motion correction and CTF estimation, was done in Scipion, followed by particle picking in crYOLO resulting 679 185 picked particles. (B) The picked particles were subject to two rounds of 2D classification ($T = 13$) to remove the obvious junk particles. (C) Selected particles were further cleaned up by a round of 3D classification ($T = 5$). (D) Particles that fall within the best 3D classes (class 1 and 2) were further refined either separately or merged together. Here, using the reconstruction from particles that belong to class 1 reached 7.4 Å; reconstruction with particles class 2 reached 4.0 Å and the merged particles from both classes reached 4.2 Å. (E) Afterwards, a second 3D classification was performed using class 2 particles, which yielded a final set of 83 278 particles. (F) After several refinement steps, the final 3D reconstruction map reached a resolution of 3.46 Å (GSFC 0.143). Structure figures were prepared using UCSF Chimera [52].

Salipro reconstitution resulted in cryo-EM structure determination of MsbA to higher resolution

With the ability to reach a higher resolution in the Salipro system, it is possible to determine the detailed coordination of Mg^{2+}-ADP and vanadate between the two NBDs of MsbA. While in the previous cryo-EM structures of MsbA many side chains could not be modelled due to limited resolution [9], the quality of our map at 3.5 Å resolution has allowed us to unambiguously model the ADP, vanadate and Mg^{2+} molecules in their binding sites located in between both NBDs (Fig. 4). The binding pocket for ADP (A) is formed by D117 (chain A), Q485 (chain B), S380 (chain A), K382 (chain A) S383 (chain A) and T384 (chain A). The aromatic residue Y351 is forming π–π stacking interactions to the adenosine. A similar interaction could be described for MsbA in liposomes with
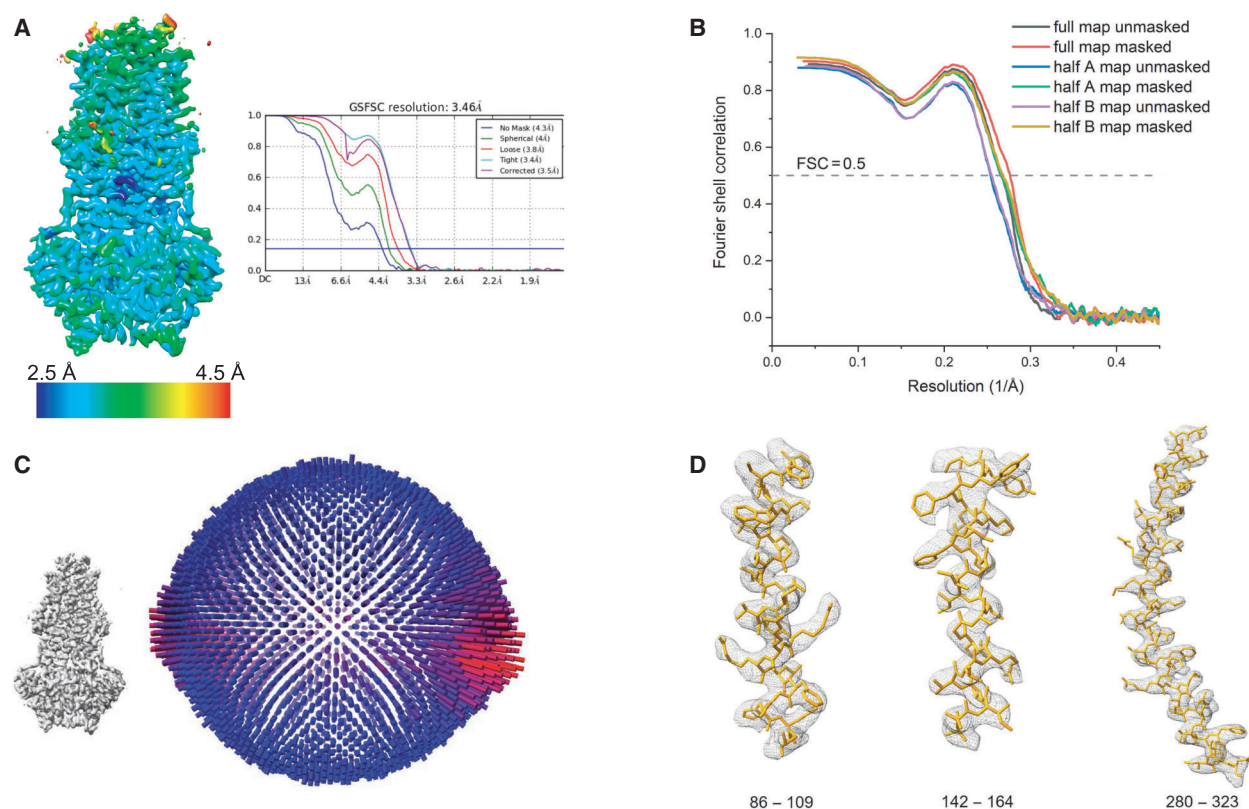
Fig. 3. Single-particle cryo-EM analysis of MsbA trapped with ADP- vanadate in Salipro. (A) Final 3D reconstitution filtered to 3.5 Å, coloured according to the local resolution and corresponding FSC plots. (B) FSC curves of the refined model versus the unmasked (black) and masked (red) full map and versus the map of half A (unmasked: blue, masked: green) and half B (unmasked: purple, masked: yellow). (C) Angular distribution of the particles included in the final reconstitution. (D) Selected cryo-EM densities (grey mesh) with the atomic model in orange. Structure figures were prepared using UCSF Chimera [52] and PYMOL.

ATP [32] and in the crystal structure with AMPPNP (pdb:3B60) [8]. Vanadate (A) is also coordinated by residues from different NBDs: A510 (chain B) and H537 (chain A), G483 (chain B), K382 (chain A), S378 (chain A) and S482 (chain B; Fig. 4C). The Mg^{2+} is coordinated between the vanadate, ADP, S383 (chain A) and Q424 (chain A). The joint coordination of ADP-Vi by residues from both NBDs locks MsbA in an occluded state.
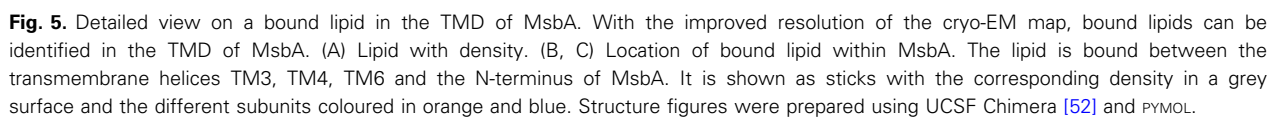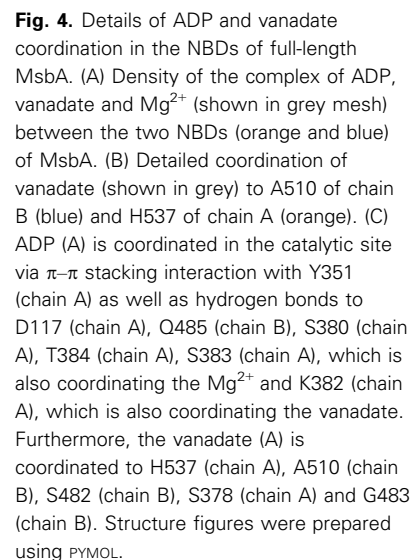
The improved resolution also allowed the modelling of a lipid bound in a conserved binding pocket between transmembrane helices TM3, TM4, TM6 and the N-terminus (Fig. 5). Interestingly, TM4 and TM6 are important for switching from apo to Vi-trapped state [33]. MsbA often co-purifies with several lipids as observed by native MS [34]. The odd positioning of the lipid could imply a stabilising role within the cavity, rather than the POPC we added during Salipro reconstitution. The stability and activity of MsbA requires the presence of directly bound lipids [30]. Interestingly, the recent cryo-EM reconstruction of MsbA with first-

generation inhibitors [35] also contains several unmodelled lipid-like densities in many pockets.

Comparison with existing MsbA structures

Several structures of MsbA in different states along the functional cycle have been determined in the last decade by X-ray crystallography or single-particle cryo-electron microscopy (cryo-EM). These structures range from inward-open conformations (pdb: 5TV4 [9], 6O30 [20], 6BL6 [20], 3B5X [8], 3B5W [8], 6BPL [19], 6BPP [19], 6UZ2 [21], 6UZL [21]) via occluded states (pdb: 5TTP [9]) to outward open conformations (pdb: 3B5Y [9], 3B60 [9], 3B5Z [9]). Our structure of MsbA with Mg^{2+}-ADP-Vi in Salipro can be classified as an occluded state and is most similar to the previously determined occluded model in nanodiscs (pdb: 5TTP) (Fig. 6).

Several structures of MsbA have been previously reported in ADP-vanadate trapped states. One was the cryo-EM structure of MsbA with ADP-vanadate in nanodiscs (pdb:5TTP), determined at 4.8 Å resolution

Fig. 4. Details of ADP and vanadate coordination in the NBDs of full-length MsbA. (A) Density of the complex of ADP, vanadate and Mg^{2+} (shown in grey mesh) between the two NBDs (orange and blue) of MsbA. (B) Detailed coordination of vanadate (shown in grey) to A510 of chain B (blue) and H537 of chain A (orange). (C) ADP (A) is coordinated in the catalytic site via π–π stacking interaction with Y351 (chain A) as well as hydrogen bonds to D117 (chain A), Q485 (chain B), S380 (chain A), T384 (chain A), S383 (chain A), which is also coordinating the Mg^{2+} and K382 (chain A), which is also coordinating the vanadate. Furthermore, the vanadate (A) is coordinated to H537 (chain A), A510 (chain B), S482 (chain B), S378 (chain A) and G483 (chain B). Structure figures were prepared using PYMOL.

Fig. 5. Detailed view on a bound lipid in the TMD of MsbA. With the improved resolution of the cryo-EM map, bound lipids can be identified in the TMD of MsbA. (A) Lipid with density. (B, C) Location of bound lipid within MsbA. The lipid is bound between the transmembrane helices TM3, TM4, TM6 and the N-terminus of MsbA. It is shown as sticks with the corresponding density in a grey surface and the different subunits coloured in orange and blue. Structure figures were prepared using UCSF Chimera [52] and PYMOL.

[9]. In this structure, neither amino acid side chains nor ADP-Vi could be modelled due to limited resolution. Apart from the improved resolution and occupied nucleotide binding site, we see just minor differences to our structure in Salipro (RMSD: 2.4 Å; Fig. 6A). The other models include a crystal structure of ADP-vanadate trapped MsbA from *Salmonella typhimurium* determined to 4.2 Å, which only allowed modelling of

the protein backbone as dummy atoms (pdb:3B5Z), and the crystal structure of AMPPNP-bound MsbA (pdb:3B60) [8]. For these structures the protein was crystallised in undecyl-ß-D-maltoside detergent. Interestingly, these crystal structures show significant differences in the orientation of the transmembrane helices in particular on the periplasmic side (Fig. 6A) compared to both cryo-EM structures in lipidic environment
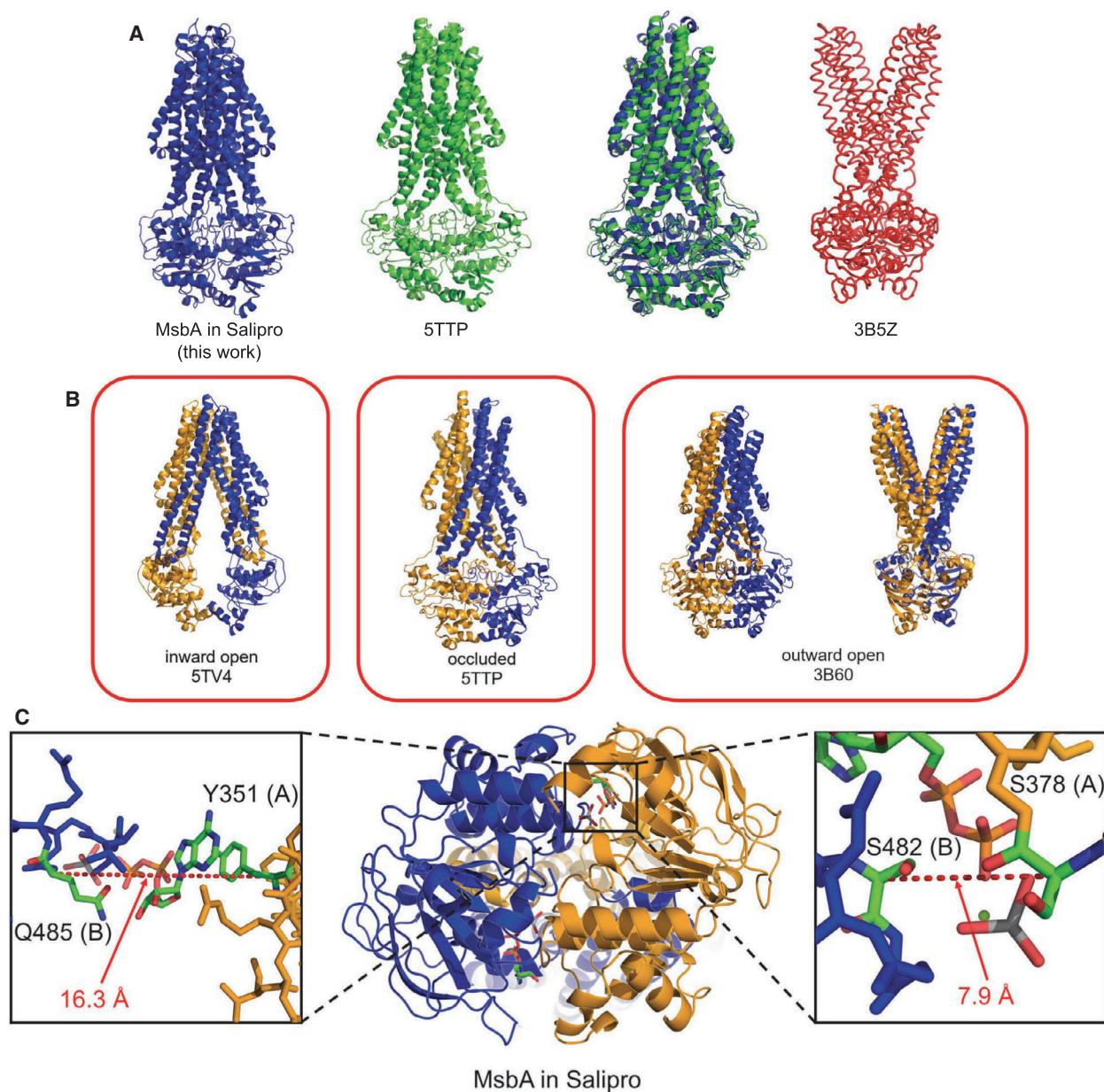
Fig. 6. Comparison of Salipro-reconstituted MsbA (ADP-Vi) with existing MsbA structures. (A) Comparison of ADP-Vi-bound MsbA structures reconstituted in Salipro (this study, blue) and nanodiscs (pdb: 5TTP, green) [9] as well as with the crystal structure of ADP-Vi-bound MsbA in detergent in outward-facing state (pdb: 3B5Z, red) [8]. (B) The structure of MsbA in nanodiscs without nucleotides shows an inward open state (pdb: 5TV4) [9], while the addition of ADP-vanadate leads to an occluded state of the protein (5TTP) [9]. MsbA in detergent in complex with AMPPNP adopts an outward open state (3B60) [8]. MsbA in Salipro and ADP-vanadate (this study) also adopts an occluded state. (C) View from the cytoplasm to the ADP-Vi-bound MsbA structure in Salipro with C-alpha distances between S482 (Walker A motif) and S378 (signature motif) in opposing NBD. Furthermore, the C-alpha distance between Y351 and Q485 from the different chains is shown. Structure figures were prepared using PYMOL.

(pdb:5TTP and this structure) and can be classified as outward-open conformation. It is tempting to speculate that the higher flexibility in detergent allows MsbA to transition to the outward-open state while in nanodiscs and saposins it is harder to reach this conformation.

For efficient nucleotide binding and hydrolysis in ABC transporters the Walker A and signature motifs from opposing NBDs have to come together [36]. The C-alpha distances between S482 (Walker A motif) and S378 (signature motif) in the opposing NBD are 7.9 Å

for our (occluded state) structure in Salipro (Fig. 6C), 6.2 Å for the ADP-Vi-bound (occluded state) cryo-EM structure in nanodiscs (pdb:5TTP) [9], 6.0 Å for the ADP-Vi-bound and 7.5 Å for the AMPPNP-bound (outward-open) crystal structures, respectively, in detergent (pdb:3B5Z/3B60) [8]. Similarly, the distance of the C-alpha atoms of Y351 (A) and Q485 (B) is 16.3 Å in Salipro (Fig. 6C), 15.8 Å for 5TTP [9] and 18.0/16.8 Å for 3B5Z/3B60 [8], indicating a similar and optimal orientation of the NBDs for nucleotide binding, details of which could now be visualized with our improved resolution obtained by Salipro-reconstitution. The comparison with the AMPPNP-bound crystal structure of MsbA [8] (pdb:3B60) in outward-open conformation reveals only minor differences with respect to the NBDs (RMSD: 1.0 Å). The side chain of Glu424 coordinates the Mg^{2+} in our structure, while it adopts a different rotamer in pdb:3B60. Overall, the nucleotide-binding pocket is slightly more closed in our structure compared to AMPPNP-bound state, due to a different orientation of loop T350-P357. The similarity between NBD distances of different states indicates that the switch in the transmembrane region between occluded and outward-open conformations of ADP-Vi-bound states is not accompanied by major rearrangements of the NBDs.

The reason why our reconstitution in Salipro resulted in a significantly improved resolution for the ADP-Vi-bound state of MsbA compared to other reconstitution systems is still not understood. One possibility would be that MsbA is less dynamic in Salipro (when trapped with ADP-Vi). As these effects, however, are difficult to predict our results further illustrate that many reconstitution systems should be tried for improving the resolution of any membrane protein of interest.

Materials and methods

Materials

Detergents and lipids were purchased from the following companies: DDM (#D310/Anatrace), cholate (#3407.1/Roth), POPC (#850457P/Avanti Polar Lipids). All other chemicals were of analytical grade and obtained from Roth (Karlsruhe, Germany) or Sigma Aldrich/Merck (Darmstadt, Germany). MsbA and Salipro were produced in ILL's Life Sciences Group [37] as described below.

Protein expression and purification

MsbA was expressed and purified as previously described [16]. Briefly, MsbA (from *E. coli*) containing an N-terminal His$_6$-tag in a pNEK vector was expressed in the *E. coli* strain C43 (DE3) and grown in 2× TY medium at 37 °C. At an OD$_{600}$ of 1.5, the temperature was decreased to 20 °C and protein expression was induced with 0.1 mM isopropyl ß-D-1-thiogalactopyranoside (IPTG) overnight. Cells were harvested and resuspended in lysis buffer (30 mM Tris pH: 8, 300 mM NaCl, 10% glycerol, 5 mM MgCl$_2$) and disrupted in four cycles in a high-pressure homogenizer (EmulsiFlex-C3; Avestin, Ottawa, ON, Canada). After centrifugation (20 000 *g*, 25 min, 4 °C) the supernatant was spun down at 100 000 *g* for 100 min at 4 °C to obtain the membrane fractions. Membranes were solubilised in 1% (w/v) DDM, 30 mM Tris (pH 8), 300 mM NaCl, 10% glycerol, 10 mM imidazole and gently stirred for 90 min at 4 °C. For the purification of MsbA pre-equilibrated Ni-nitrilotriacetic acid (Ni-NTA) resin was added to the solubilised protein and incubated for 60 min at 4 °C. The resin was washed with washing buffers with an increasing imidazole concentration (0.03% DDM, 30 mM Tris pH: 8, 300 mM NaCl, 10/30 mM imidazole), and the purified MsbA was eluted [0.03% DDM, 30 mM Tris (pH 8), 300 mM NaCl, 400 mM imidazole]. Fractions containing MsbA were pooled and concentrated to 2–5 mg·mL^{-1} before reconstitution into Salipro.

Saposin A in a pNIC28-Bsa4 vector was expressed with an N-terminal His$_6$-tag and tobacco etch virus (TEV) cleavage site in the *E. coli* strain Rosetta-gami 2 [22] and grown in terrific broth (TB) media at 37 °C until an OD$_{600}$ of 1.5 was reached. The temperature was lowered to 20 °C, and 0.1 mM IPTG was added for an overnight induction. After harvesting the cells, the pellet was resuspended in lysis buffer (20 mM sodium phosphate (pH 7.4), 300 mM NaCl, 5% glycerol, 15 mM imidazole) and the cells were lysed via sonication. The cell suspension was heated to 70 °C for 20 min to precipitate all thermolabile components. After a centrifugation step (16 000 *g*, 20 min, 4 °C) an immobilized metal affinity chromatography (IMAC) step was performed to purify SapA. Pre-equilibrated Ni-NTA resin was added to the supernatant of the centrifugation step and gently mixed for 90 min at 4 °C. The resin was washed, and the protein eluted with buffers with an increasing imidazole concentration (20 mM sodium phosphate (pH 7.4), 300 mM NaCl, 5% glycerol, 30/400 mM imidazole). TEV-protease was added to the eluted protein and dialysed overnight at 4 °C against dialysis buffer (20 mM sodium phosphate (pH 7.4), 300 mM NaCl, 5% glycerol, 1 mM DTT). In a second IMAC step, the TEV-protease and the cleaved His$_6$-tag were removed. The cleaved protein was concentrated and applied to an S75 16/600 (GE Healthcare, Chicago, IL, USA) column [size-exclusion chromatography (SEC) buffer: 20 mM HEPES, pH 7.4, 200 mM NaCl] to perform a SEC to yield the pure SapA. The protein was concentrated and stored at −80 °C.

Reconstitution of MsbA in Salipro

Reconstitution of MsbA into Salipro was performed similar as previously described [30]. Briefly, POPC was

resuspended from a dry lipid film in 100 mM cholate to obtain a 50 mM lipid stock solution. For the reconstitution of MsbA in Salipro the molar ration of 1 : 4 : 20 (MsbA : SapA : POPC) in buffer containing 20 mM HEPES, pH 7.4, 200 mM NaCl was mixed and incubated at 4 °C for 30 min. The Salipro formation was initiated by adding 0.8 g·mL^{-1} equilibrated biobeads and under constant agitation overnight at 4 °C. The reconstituted MsbA was extracted from the biobeads, concentrated and purified on a S200 column (GE Healthcare) in a buffer containing 20 mM HEPES, pH 7.4, 200 mM NaCl.

MsbA activity assay

MsbA activity was measured in Salipro using the Baginski assay [38,39], similar as previously described [30,40]. About 5 μg MsbA in Salipro in a buffer containing 30 mM Tris (pH 7.5), 150 mM NaCl and 5 mM MgCl$_2$ were incubated in 50 μL with different ATP concentrations (0/100/200/300/ 500/1000/2000/4000 μM) for 12 min at room temperature (RT) before the reaction was stopped by adding 50 μL ascorbic acid solution (140 mM ascorbic acid, 0.5 M HCl, 0.1% SDS, 5 mM ammonium heptamolybdate). The addition of 75 μL solution B (75 mM sodium citrate, 2% (w/v) sodium metaarsenite and 2% (v/v) acetic acid) was used to stop the colorimetric reaction and the absorbance at 860 nm was detected using a Tecan Infinite200 microplate reader after 20 min. All experiments were performed as biological triplicates.

Differential scanning fluorimetry (nDSF)

Thermal protein unfolding was measured by differential fluorescence fluorimetry using a nanoDSF instrument (Prometheus, NanoTemper Technologies, Munich, Germany) that monitors intrinsic tryptophan fluorescence. Protein and ligand concentrations were 0.5 mg·mL^{-1} and 0.5 mM, respectively, in 10 mM HEPES, pH 7.4, 150 mM NaCl, 5 mM MgCl$_2$ buffer. The ADP-Vi state was prepared in a forward reaction by mixing ATP and vanadate and incubating the sample for 2–3 h. A thermal gradient from 20 to 90 °C with a heating rate of 1 °C·min^{-1} was applied. All measurements were performed in duplicates. The ratio was calculated from fluorescence intensities measured at 350 and 330 nm.

Small-angle X-ray scattering

The analysis of MsbA incorporated into Salipro nanoparticles in the apo and the ADP-Vi state by SAXS was performed at the Bio-SAXS beamline P12 [41] on the storage ring PETRA III (DESY, Hamburg, Germany). All measurements were performed at 10 °C in 20 mM HEPES, pH 7.4, 200 mM NaCl, with protein concentrations of 1–5 mg·mL^{-1}. The normalization and the background

subtraction were performed by the automatic procedures on the beamline [42]. The radii of gyration were extracted by the Guinier approximation. The program GNOM [43] was used to calculate the distance distribution function ($P(r)$) and the maximal protein dimension (D_{max}) from the scattering curve.

Cryo-EM grid preparation

To the purified MsbA sample, 1 mM vanadate, 1 mM ATP and 1 mM MgCl$_2$ were added and incubated for 3 days at 4 °C. The sample was prepared for cryo-EM by applying 4 μL of the sample (0.6 mg·mL^{-1}) to a glow-discharged Quantifoil holey carbon grid R2/2 (CU, 200 mesh). The grids were blotted with filter paper and plunge-frozen in liquid ethane using an FEI Vitrobot Mark IV (Thermo Fisher Scientific Ltd, Waltham, MA, USA) with zero blot force, 6 s blot time at 4 °C and 95% humidity.

Cryo-EM data acquisition

Cryo-EM data were collected on the Titan Krios microscope at the ESRF [44] operated at 300 kV using EPU

Table 2. cryo-EM data collection and refinement statistics

	EMDB: 12145 PDB: 7BCW
Data	
Magnification	165 000
Voltage (kV)	300
Electron exposure (e$^-$/Å^2)	39.55
Defocus range (μm)	−0.8 to −3.0
Pixel size (Å)	0.827
Symmetry imposed	C2
Final particle images (no.)	83278
GS-FSC resolution at 0.143 (Å)	3.5
Initial model used	PDB 5TTP
Map sharpening *B* factor (Å^2)	−94
Model	
FSC model (0/0.143/0.5)	3.0/3.3/3.6
Nonhydrogen atoms	9023
Protein residues	1148
Ligands	VO4 (2)
	POV (2)
	ADP (2)
Bond (RMSD)	
Length (Å)	0.005
Angles (°)	0.663
MolProbity score	1.77
Clash Score	9.26
Rotamers outliers (%)	0
Ramachandran Plot	
Favored (%)	95.72
Allowed (%)	4.28
Outliers (%)	0
EMRinger score	2.27

(Thermo Fisher Scientific) equipped with a Quantum LS energy filter and Gatan K2 summit direct electron detector. Movies were recorded in counting mode at a nominal magnification of 165 000×, corresponding to a pixel size of 0.827 Å·pixel^{-1} at the specimen level. The defocus range was set from −0.8 to −3.0 μm. The exposure time was 5 s for each movie at a dose rate of 5.42 e^{-}·pixel^{-1}·s^{-1}, accumulating to a total dosage of 39.55 e^{-}·Å^{-2} over 40 frames. A total of 10 302 movies were recorded. Data collection parameters are summarized in Table 2.

Image processing

Pre-processing was carried out in Scipion [45] using scripts implemented on CM01 at the ESRF, which perform beam induced motion correction [46] and contrast transfer function (CTF) estimation [47]. Particle picking and initial 2D classification were carried using crYOLO [48] and RELION [49], respectively, as implemented in Scipion [50]. The cleaned-up set of particles were exported and used for further processing in cryoSPARC [51]. Particles were further clean-up in a 3D classification follow by a heterogeneous refinement step to remove bad particles. The best classes were used for a non-uniform refinement (C1) and a second round of 3D classification was performed. All 3D classifications and refinements were carried out in cryoSPARC. The best resolved class was selected for particle CTF refinement followed by non-uniform refinement (C2). The final map consists of a set of 83287 particles. Post-processing and local resolution estimation were done in cryoSPARC. Refer to Fig. 2 for the cryo-EM data processing pipeline.

Model building and refinement

The coordinates of MsbA that were available from the Protein Data Bank under accession number 5TTP were used as starting model. This model was placed in the cryo-EM map using UCSF Chimera [52]. The cryo-EM map was autosharpened using PHENIX prior to model building (*B* factor: −94 Å^2). The model was rebuild and refined iteratively using Coot [53], ISOLDE [54] and the PHENIX suite [55]. The later was also used for real space refinement and model validation [56,57]. The final model is available in the protein data bank under accession number pdb:7BCW.

Acknowledgements

Conflict of interest

The authors declare no conflict of interest.

Author contributions

Investigation, DMK, DAKT, IJ, SS, MM, MH and SP; Writing, DMK, DAKT, VTF and HT; Funding acquisition and supervision, VTF and HT.

Peer Review

The peer review history for this article is available at https://publons.com/publon/10.1111/febs.16327.

Data Availability Statement

The cryo-EM map and the atomic coordinates are available in the Electron Microscopy Data Bank and the Protein Data Bank under accession number EMDB-12145 and 7BCW, respectively. All other relevant data generated during and/or analysed during the current study are available from the corresponding author on reasonable request.

References

1 Holthuis JC, Menon AK. Lipid landscapes and pipelines in membrane homeostasis. *Nature*. 2014;**510**:48–57.

2 van Meer G. Dynamic transbilayer lipid asymmetry. *Cold Spring Harb Perspect Biol*. 2011;**3**:a004671.

3 Sebastian TT, Baldridge RD, Xu P, Graham TR. Phospholipid flippases: building asymmetric membranes and transport vesicles. *Biochim Biophys Acta*. 2012;**1821**:1068–77.

4 Lyons JA, Timcenko M, Dieudonne T, Lenoir G, Nissen P. P4-ATPases: how an old dog learnt new tricks - structure and mechanism of lipid flippases. *Curr Opin Struct Biol*. 2020;**63**:65–73.

5 Doerrler WT, Gibbons HS, Raetz CR. MsbA-dependent translocation of lipids across the inner membrane of *Escherichia coli*. *J Biol Chem*. 2004;**279**:45102–9.

6 Zhou Z, White KA, Polissi A, Georgopoulos C, Raetz CR. Function of *Escherichia coli* MsbA, an essential ABC family transporter, in lipid A and phospholipid biosynthesis. *J Biol Chem*. 1998;**273**:12466–75.

7 Raetz CR, Reynolds CM, Trent MS, Bishop RE. Lipid A modification systems in gram-negative bacteria. *Annu Rev Biochem*. 2007;**76**:295–329.

8 Ward A, Reyes CL, Yu J, Roth CB, Chang G. Flexibility in the ABC transporter MsbA: Alternating access with a twist. *Proc Natl Acad Sci USA*. 2007;**104**:19005–10.

9 Mi W, Li Y, Yoon SH, Ernst RK, Walz T, Liao M. Structural basis of MsbA-mediated lipopolysaccharide transport. *Nature*. 2017;**549**:233–7.

10 Higgins CF, Linton KJ. The ATP switch model for ABC transporters. *Nat Struct Mol Biol*. 2004;**11**:918–26.

11 Zoghbi ME, Cooper RS, Altenberg GA. The lipid bilayer modulates the structure and function of an ATP-binding cassette exporter. *J Biol Chem*. 2016;**291**:4453–61.

12 Borbat PP, Surendhran K, Bortolus M, Zou P, Freed JH, McHaourab HS. Conformational motion of the ABC transporter MsbA induced by ATP hydrolysis. *PLoS Biol*. 2007;**5**:e271.

13 Doshi R, van Veen HW. Substrate binding stabilizes a pre-translocation intermediate in the ATP-binding cassette transport protein MsbA. *J Biol Chem*. 2013;**288**:21638–47.

14 Moeller A, Lee SC, Tao H, Speir JA, Chang G, Urbatsch IL, et al. Distinct conformational spectrum of homologous multidrug ABC transporters. *Structure*. 2015;**23**:450–60.

15 Moradi M, Tajkhorshid E. Mechanistic picture for conformational transition of a membrane transporter at atomic resolution. *Proc Natl Acad Sci USA*. 2013;**110**:18916–21.

16 Josts I, Niebling S, Gao Y, Levantino M, Tidow H, Monteiro D. Photocage-initiated time-resolved solution X-ray scattering investigation of protein dimerization. *IUCrJ*. 2018;**5**:667–72.

17 Josts I, Gao Y, Monteiro DCF, Niebling S, Nitsche J, Veith K, et al. Structural kinetics of MsbA investigated by stopped-flow time-resolved small-angle X-ray scattering. *Structure*. 2020;**28**:348–54.e3.

18 Terakado K, Kodan A, Nakano H, Kimura Y, Ueda K, Nakatsu T, et al. Deleting two C-terminal alpha-helices is effective to crystallize the bacterial ABC transporter *Escherichia coli* MsbA complexed with AMP-PNP. *Acta Crystallogr D Biol Crystallogr*. 2010;**66**:319–23.

19 Ho H, Miu A, Alexander MK, Garcia NK, Oh A, Zilberleyb I, et al. Structural basis for dual-mode inhibition of the ABC transporter MsbA. *Nature*. 2018;**557**:196–201.

20 Padayatti PS, Lee SC, Stanfield RL, Wen PC, Tajkhorshid E, Wilson IA, et al. Structural insights into the lipid A transport pathway in MsbA. *Structure*. 2019;**27**:1114–23.e3.

21 Angiulli G, Dhupar HS, Suzuki H, Wason IS, Duong Van Hoa F, Walz T. New approach for membrane protein reconstitution into peptidiscs and basis for their adaptability to different proteins. *Elife*. 2020;**9**:e53530. https://doi.org/10.7554/eLife.53530

22 Frauenfeld J, Loving R, Armache JP, Sonnen AF, Guettou F, Moberg P, et al. A saposin-lipoprotein nanoparticle system for membrane proteins. *Nat Methods*. 2016;**13**:345–51.

23 Flayhan A, Mertens HDT, Ural-Blimke Y, Martinez Molledo M, Svergun DI, Low C. Saposin lipid nanoparticles: a highly versatile and modular tool for membrane protein research. *Structure*. 2018;**26**:345–55.e5

24 Lyons JA, Boggild A, Nissen P, Frauenfeld J. Saposin-lipoprotein scaffolds for structure determination of membrane transporters. *Methods Enzymol*. 2017;**594**:85–99.

25 Kim JJ, Gharpure A, Teng J, Zhuang Y, Howard RJ, Zhu S, et al. Shared structural mechanisms of general anaesthetics and benzodiazepines. *Nature*. 2020;**585**:303–8.

26 Nguyen NX, Armache JP, Lee C, Yang Y, Zeng W, Mootha VK, et al. Cryo-EM structure of a fungal mitochondrial calcium uniporter. *Nature*. 2018;**559**:570–4.

27 Rahman MM, Teng J, Worrell BT, Noviello CM, Lee M, Karlin A, et al. Structure of the native muscle-type nicotinic receptor and inhibition by snake venom toxins. *Neuron*. 2020;**106**:952–62.e5.

28 Gharpure A, Teng J, Zhuang Y, Noviello CM, Walsh RM Jr, Cabuco R, et al. Agonist selectivity and ion permeation in the alpha3beta4 ganglionic nicotinic receptor. *Neuron*. 2019;**104**:501–11.e6.

29 Kintzer AF, Green EM, Dominik PK, Bridges M, Armache JP, Deneka D, et al. Structural basis for activation of voltage sensor domains in an ion channel TPC1. *Proc Natl Acad Sci USA*. 2018;**115**:E9095–104.

30 Kehlenbeck DM, Josts I, Nitsche J, Busch S, Forsyth VT, Tidow H. Comparison of lipidic carrier systems for integral membrane proteins - MsbA as case study. *Biol Chem*. 2019;**400**:1509–18.

31 Josts I, Nitsche J, Maric S, Mertens HD, Moulin M, Haertlein M, et al. Conformational states of ABC transporter MsbA in a lipid environment investigated by small-angle scattering using stealth carrier nanodiscs. *Structure*. 2018;**26**:1072–9.e4.

32 Kaur H, Abreu B, Akhmetzyanov D, Lakatos-Karoly A, Soares CM, Prisner T, et al. Unexplored nucleotide binding modes for the ABC exporter MsbA. *J Am Chem Soc*. 2018;**140**:14112–25.

33 Spadaccini R, Kaur H, Becker-Baldus J, Glaubitz C. The effect of drug binding on specific sites in transmembrane helices 4 and 6 of the ABC exporter MsbA studied by DNP-enhanced solid-state NMR. *Biochim Biophys Acta Biomembr*. 2018;**1860**:833–40.

34 Gupta K, Li J, Liko I, Gault J, Bechara C, Wu D, et al. Identifying key membrane protein lipid interactions using mass spectrometry. *Nat Protoc*. 2018;**13**:1106–20.

35 Thelot FA, Zhang W, Song K, Xu C, Huang J, Liao M. Distinct allosteric mechanisms of first-generation MsbA inhibitors. *Science*. 2021;**374**:580–5.

36 Chen J. Molecular mechanism of the *Escherichia coli* maltose transporter. *Curr Opin Struct Biol*. 2013;**23**:492–8.

37 Haertlein M, Moulin M, Devos JM, Laux V, Dunne O, Forsyth VT. Biomolecular deuteration for neutron structural biology and dynamics. *Methods Enzymol*. 2016;**566**:113–57.

38 Baginski ES, Epstein E, Zak B. Review of phosphate methodologies. *Ann Clin Lab Sci*. 1975;**5**:399–416.

39 Chifflet S, Torriglia A, Chiesa R, Tolosa S. A method for the determination of inorganic phosphate in the presence of labile organic phosphate and high concentrations of protein: application to lens ATPases. *Anal Biochem*. 1988;**168**:1–4.

40 Nitsche J, Josts I, Heidemann J, Mertens HD, Maric S, Moulin M, et al. Structural basis for activation of plasma-membrane Ca(2+)-ATPase by calmodulin. *Commun Biol*. 2018;**1**:206.

41 Blanchet CE, Spilotros A, Schwemmer F, Graewert MA, Kikhney A, Jeffries CM, et al. Versatile sample environments and automation for biological solution X-ray scattering experiments at the P12 beamline (PETRA III, DESY). *J Appl Crystallogr*. 2015;**48**:431–43.

42 Konarev PV, Volkov VV, Sokolova AV, Koch MHJ, Svergun DI. PRIMUS: a Windows PC-based system for small-angle scattering data analysis. *J Appl Crystallogr*. 2003;**36**:1277–82.

43 Svergun DI. Determination of the regularization parameter in indirect-transform methods using perceptual criteria. *J Appl Crystallogr*. 1992;**25**:495–503.

44 Kandiah E, Giraud T, de Maria Antolinos A, Dobias F, Effantin G, Flot D, et al. CM01: a facility for cryo-electron microscopy at the European synchrotron. *Acta Crystallogr D Struct Biol*. 2019;**75**:528–35.

45 Maluenda D, Majtner T, Horvath P, Vilas JL, Jimenez-Moreno A, Mota J, et al. Flexible workflows for on-the-fly electron-microscopy single-particle image processing using Scipion. *Acta Crystallogr D Struct Biol*. 2019;**75**:882–94.

46 Zheng SQ, Palovcak E, Armache JP, Verba KA, Cheng Y, Agard DA. MotionCor2: anisotropic correction of beam-induced motion for improved cryo-electron microscopy. *Nat Methods*. 2017;**14**:331–2.

47 Zhang K. Gctf: Real-time CTF determination and correction. *J Struct Biol*. 2016;**193**:1–12.

48 Wagner T, Merino F, Stabrin M, Moriya T, Antoni C, Apelbaum A, et al. SPHIRE-crYOLO is a fast and accurate fully automated particle picker for cryo-EM. *Commun Biol*. 2019;**2**:218.

49 Zivanov J, Nakane T, Forsberg BO, Kimanius D, Hagen WJ, Lindahl E, et al. New tools for automated high-resolution cryo-EM structure determination in RELION-3. *Elife*. 2018;**7**:e42166. https://doi.org/10.7554/eLife.42166

50 de la Rosa-Trevin JM, Quintana A, Del Cano L, Zaldivar A, Foche I, Gutierrez J, et al. Scipion: a software framework toward integration, reproducibility and validation in 3D electron microscopy. *J Struct Biol*. 2016;**195**:93–9.

51 Punjani A, Rubinstein JL, Fleet DJ, Brubaker MA. cryoSPARC: algorithms for rapid unsupervised cryo-EM structure determination. *Nat Methods*. 2017;**14**:290–6.

52 Pettersen EF, Goddard TD, Huang CC, Meng EC, Couch GS, Croll TI, et al. UCSF ChimeraX: structure visualization for researchers, educators, and developers. *Protein Sci*. 2021;**30**:70–82.

53 Emsley P, Lohkamp B, Scott WG, Cowtan K. Features and development of Coot. *Acta Crystallogr D Biol Crystallogr*. 2010;**66**:486–501.

54 Croll TI. ISOLDE: a physically realistic environment for model building into low-resolution electron-density maps. *Acta Crystallogr D Struct Biol*. 2018;**74**:519–30.

55 Liebschner D, Afonine PV, Baker ML, Bunkoczi G, Chen VB, Croll TI, et al. Macromolecular structure determination using X-rays, neutrons and electrons: recent developments in Phenix. *Acta Crystallogr D Struct Biol*. 2019;**75**:861–77.

56 Afonine PV, Klaholz BP, Moriarty NW, Poon BK, Sobolev OV, Terwilliger TC, et al. New tools for the analysis and validation of cryo-EM maps and atomic models. *Acta Crystallogr D Struct Biol*. 2018;**74**:814–40.

57 Afonine PV, Poon BK, Read RJ, Sobolev OV, Terwilliger TC, Urzhumtsev A, et al. Real-space refinement in PHENIX for cryo-EM and crystallography. *Acta Crystallogr D Struct Biol*. 2018;**74**:531–44.